Preparation and *in Vitro* Evaluation of Tamoxifen-Conjugated, Eco-Friendly, Agar-Based Hybrid Magnetic Nanoparticles for Their Potential Use in Breast Cancer Treatment

Zanib Khan, Sadia Sattar, Muhammad Abubakar, Muhammad Javed Arshed, Roohi Aslam, Syed Tahir Abbas Shah, Sundus Javed, Aamira Tariq, Shumaila Manzoor, and Nazish Bostan*
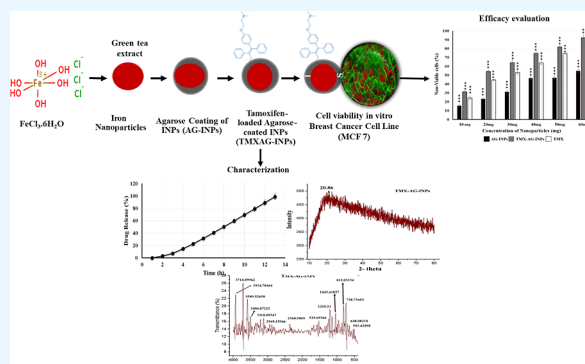
Read Online

ACCESS | Metrics & More | Article Recommendations

ABSTRACT: Tamoxifen is the drug of choice as hormonal therapy for hormone receptor-positive breast cancers and can reduce the risk of breast cancer recurrence. However, oral tamoxifen has a low bioavailability due to liver and intestinal metabolic passes. To overcome this problem and utilize the potential of this drug to its maximum, inorganic nanoparticle carriers have been exploited and tested to increase its bioavailability. Biocompatibility and unique magnetic properties make iron oxide nanoparticles an excellent choice as a drug delivery system. In this study, we developed and tested a "green synthesis" approach to synthesize iron nanoparticles from green tea extract and coated them with agar for longer stability (AG-INPs). Later, these hybrid nanoparticles were conjugated with tamoxifen (TMX). By using this approach, we synthesized stable agar-coated tamoxifen-conjugated iron nanoparticles (TMX-AG-INPs) and characterized them with Fourier-transform infrared (FTIR) spectroscopy. The average particle size of AG-INPs was 26.8 nm, while the average particle size of tamoxifen-loaded iron nanoparticles, TMX-AG-INPs, was 32.1 nm, as measured by transmission and scanning electron microscopy. The entrapment efficiency of TMX-AG-INPs obtained by the drug release profile was 88%, with a drug loading capacity of 43.5%. TMX-AG-INPs were significantly ($p < 0.001$) efficient in killing breast cancer cells when tested *in vitro* on the established breast cancer cell line MCF-7 by cell viability assay, indicating their potential to control cell proliferation.

1. INTRODUCTION

Breast cancer is one of the most common cancers found in women and is a leading cause of cancer-related deaths[1] (WHO, 2019). In 2020, roughly 2.3 million cases of breast cancer have been reported, with an estimated death toll of 0.69 million. As predicted by the International Agency for Research on Cancer (IARC), the global burden of breast cancer is likely to exceed 3 million cases per year by 2040, with an estimated 1 million deaths per year. Breast cancer is treated with a variety of chemotherapeutic drugs.[2] Existing anticancer drugs do not distinguish between malignant and normal cells well, resulting in systemic toxicity and side effects.[3] The drug's maximum permitted dose is severely limited because of this toxicity. In addition, poor distribution, rapid clearance, and drug penetration into cancer cells from traditional formulations are limiting. Succinctly, because of the widespread dispersion and rapid removal of the medication from targeted organs, treatment requires heavy doses that lead to greater toxicity and are economically challenging.[4]

Tamoxifen (TMX) is one of the most commonly used medications for estrogen-receptor-positive breast cancer at all stages. It is the first anticancer medicine approved for the prevention of breast cancer in high-risk women. It has been shown to reduce breast cancer incidence in both pre- and postmenopausal patients.[5,6] However, it comes with a price, and long-term treatment with TMX can cause thrombocytopenia, leucopenia, hemolytic anemia, hepatic necrosis, multifocal hepatic fatty infiltration, oxidative stress-mediated hepatotoxicity, and endometrial cancer. Free tamoxifen can diffuse nonspecifically and hence produce unwanted toxicity. One of the biggest problems in chemotherapy for solid tumors is targeted drug delivery to the solid tumor tissue, avoiding unwanted toxicity in surrounding tissue while maintaining effective concentration in the tumor. This can be achieved by

exploiting the enhanced permeability retention (EPR) effect that allows selective accumulation and retention of macromolecules of certain sizes in tumor cells compared to surrounding healthy tissue, achieving targeted drug delivery.[7] TMX can be loaded onto these nanocarriers for safer and more effective solid tumor treatment. This can maximize the benefits of the drug with minimum toxicity by providing targeted delivery to specific tissue.[8]

The incorporation of TMX into nanoparticles allows its gradual release in low concentrations over a prolonged period of time, which greatly reduces the dose-dependent toxicity of tamoxifen.[9] Moreover, the desired therapeutic efficacy of tamoxifen can be achieved if the required concentration of an active drug reaches its target site.[10] Even though the drug is provided in optimum concentrations, the active drug may be less due to the protective mechanisms of the body or the presence of macrophages from the reticuloendothelial system and tumor-associated macrophages, which destroy TMX or foreign molecules.[11] Therefore, nanocarriers, in addition to delivering TMX at a smaller and safer dose to tumors, can also protect hydrophobic TMX molecules from degradation by macrophages during their transportation within the blood. It increases drug circulation time, which enables the required concentration of TMX to reach tumor site.[9,11] It is evident from the literature that 1−5% of nanoformulated drugs can accumulate in target tissues in comparison to 0.01% of free drugs reaching the target tissue.[12] These nanoscale drug delivery systems are crucial for targeted drug delivery to tumor tissue, allowing maximum exploitation of the tumor microenvironment for selective drug administration through the EPR effect.[12−14]

Magnetic iron oxide nanoparticles (MINPs) have proven efficacy as targeted drug delivery systems. Owing to their surface properties, they can be easily conjugated with a variety of materials for targeted therapeutics; however, their high surface energy enables them to aggregate and interact nonspecifically with plasma proteins, resulting in immune opsonization and rapid clearance of these particles from the system. This drawback can be eliminated by surface coating of these iron nanoparticles with some non-toxic material that is biocompatible. This coating improves MINP drug loading (DL) capacity as well as stability and efficacy in targeted cells. One such example is TMX-loaded tyrosine-modified Fe_3O_4 magnetic NPs that have been evaluated for their biocompatibility, entrapment efficacy, TMX release profile, and anticancer activity on MCF-7 cell lines.[15] In this context, we have designed this study to produce MINPs with green tea extract, coat them with agar (a carbohydrate), and evaluate them.

Because of their promising *in vitro* results and ease of usage, protein-based nanoparticles have also played an important role as drug carriers and anti-cancer representatives. In the present study, tamoxifen-loaded carb-coated iron nanoparticles were synthesized and characterized, and the *in vitro* effectiveness of the formulation was evaluated.

2. MATERIALS AND METHODS

2.1. Synthesis and Coating of Green Nanoparticles.
Ferric chloride hexahydrate ($FeCl_3 \cdot 6H_2O$, Sigma-Aldrich, cat no. 236489) was used as a precursor to produce nanoparticles. Briefly, a 0.1 M solution of $FeCl_3 \cdot 6H_2O$ was prepared in 150 mL of deionized distilled water by dissolving 4.054 g of $FeCl_3 \cdot 6H_2O$. Meanwhile, the green tea extract was prepared from

commercial tea obtained from a retail shop. The extract was prepared by heating 10 g of green tea leaves in 500 mL of distilled water at 95 °C in a water bath (Memmert, WNB) for 1 h. Later, the extract was filtered with a CYTIVA Whatman fluted filter paper (Sigma-Aldrich GB003, cat no. WHA10427810) and stored at 4 °C until further use. $FeCl_3 \cdot 6H_2O$ was reduced by adding green tea extract dropwise to 0.1 M $FeCl_3 \cdot 6H_2O$ solution in a ratio of 1:1 with continuous stirring for 30 min. $FeCl_3 \cdot 6H_2O$ changes color from yellow-brown to black upon reduction. The prepared nanoparticles were separated by a magnet for 10 min. Next, these iron oxide nanoparticles (INPs) were coated with agar (Merck, Millipore cat no. 101614). Briefly, a 10% agar solution (w/v) was prepared in 100 mL of deionized distilled water (dH_2O) and heated at 95 °C for 2 h. The agar was poured onto Petri plates and solidified into discs. These discs were immersed in a solution of INPs for 24 h. Later, these discs were washed with deionized distilled water. A second wash was performed using 2 M NaOH (sodium hydroxide; Merck, Millipore cat no. 106462), and then the discs were washed again 3 times using dH_2O. The agar discs were dried for 24 h under a vacuum and ground into powder. The magnetic property of these agar-coated iron nanoparticles (AG-INPs) was confirmed by a magnet.

2.2. Iron Nanoparticle Loading with Tamoxifen.
Tamoxifen-loaded agar-coated iron nanoparticles (TMX-AG-INPs) were prepared by the single emulsion method as described by Chevalier,[16] followed by solvent evaporations with a few modifications. Briefly, a tamoxifen citrate salt (Sigma-Aldrich, cat no. T9262) solution is prepared by dissolving 2.5 mg of salt in 2 mL of ethanol. Whereas, the AG-INP solution was prepared by dissolving 10 mg AG-INPs in 3 mL of dH_2O. These two were mixed in a ratio of 1:2 and magnetically stirred at room temperature for 24 h in the dark to get an emulsion and complete solvent evaporation. The resultant TMX-AG-INPs were collected by centrifugation at 14,000 rpm separated, by an external magnet (1.3 T), and dried at 80 °C for 6 h.

2.3. Entrapment Efficiency and Drug Loading.
To determine DL efficiency, 5 mg of TMX-AG-INPs was dissolved in 10 mL of ethanol and placed in a shaking incubator for 24 h at 37 °C. After incubation, the particles were placed on a magnetic plate for settlement. The collected supernatant was diluted by using phosphate-buffered saline (PBS) solution, and the absorbance of the supernatant was measured by UV−vis-spectroscopy (Hitachi, Japan, U-2010 spectrophotometer) at 278 nm.[15] Then, drug entrapment and loading efficiency were measured against each value of absorbance using a TMX calibration curve, and loading capabilities were measured by using the following formulae.

$$\% \, DL = \frac{\text{amount of entrapped drug in nanoparticles (\% EE)}}{\text{total weight of iron nanoparticles}} \times 100$$

$$\% \, EE = [(\text{weight of tamoxifen coated iron nanoparticles} - \text{drug in supernatant})/(\text{total drug})] \times 100$$

2.4. Tamoxifen Release Evaluation.
To determine *in vitro* drug release 5 mg of the TMX-AG-INPs were dissolved in 30 mL of PBS (phosphate-buffered solution) and incubated at 37 °C. After each hour, 1 mL of the sample was drawn, and the absorbance was measured by spectroscopy at 278 nm. Fresh PBS was replaced in the original solution. At each time point,
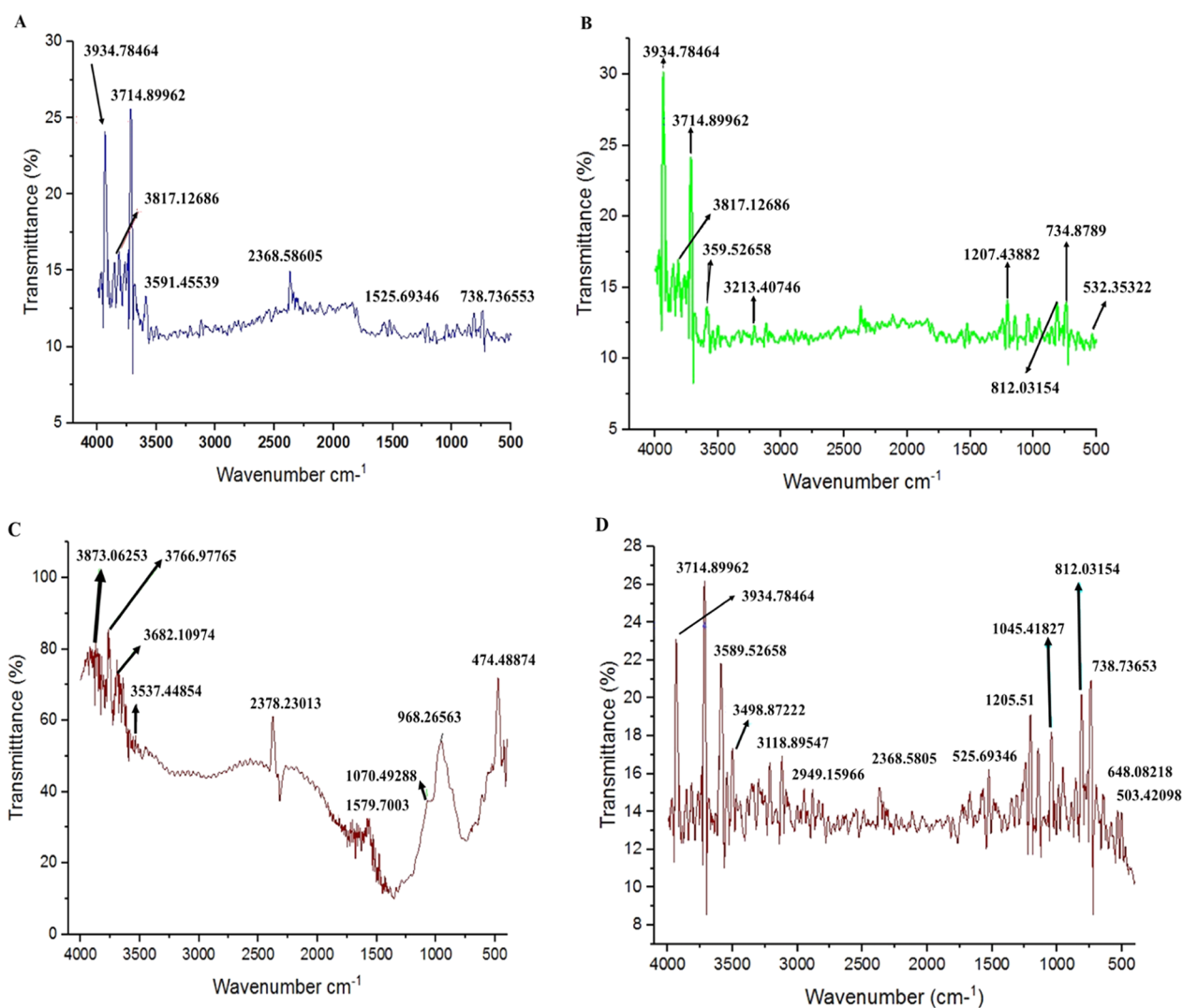
Figure 1. FTIR spectra of (A) INPs, (B) AG-INPs, (C) tamoxifen (TMX) alone, and (D) TMX-AG-INPs is given.

two readings were taken, and the average of these readings was used to calculate the concentration of free drug for 12 h.

2.5. Evaluation of Anticancer Activity. To evaluate the capacity of TMX-AG-INPs for anticancer activity, the breast cancer cell line MCF-7 was used. This is a standard breast cancer cell line (Sigma-Aldrich CB_86012803) of human breast adenocarcinoma. MCF-7 (Michigan Cancer Foundation-7) was maintained in Dulbecco's modified Eagle medium (DMEM, Thermo Scientific cat no. 11965084) containing 10% fetal bovine serum (FBS; Thermo Scientific cat no. A4766801) at 37 °C in a 5% CO_2 incubator. From master stock, the culture media was discarded, and MCF-7 cells were trypsinized with 0.25% trypsin and resuspended in fresh culture media (DMEM), as described by Jayashree.[17]

2.6. Cell Viability Assay by the Dye Exclusion Test. The number of viable cells in any suspension can be determined by the dye exclusion test. Live cells have intact plasma membranes that do not allow certain dyes such as Trypan blue (Thermo Scientific cat no. 15250061) to pass through, whereas non-viable cells have damaged membranes, hence their cytoplasm colors blue with dye. The dye exclusion test is used to determine the number of viable cells present in a cell suspension. To perform this test, sterilized Eppendorf tubes (1.5 mL) were seeded with 1×10^4 cells in 1 mL and

incubated in a CO_2 chamber overnight at 37 °C. The next day, the culture media was aspirated, and cells attached to the walls were treated with different concentrations (10, 20, 30, 40, 50, and 60 mg/mL) of INPs, TMX-AG-INPs, and TMX alone in 1 mL PBS. The plates were incubated for 48 h in a CO_2 chamber at 37 °C. After that, 100 μL of cell suspension dilution was taken in a separate sterilized Eppendorf tube and mixed with an equal volume of 0.4% Trypan blue. After 3−5 min of incubation, cell viability was observed on a hemacytometer. Blue-colored uptake indicated non-viable cells, whereas transparent cells indicated viable cells. The procedure was repeated in triplicates, and an average of the triplicates is used to calculate percentage viability and non-viability by using the following formula.

$$\text{\% Viability} = \text{total number of viable cells per aliqoute/total}$$
$$\text{cells in an aliquot} \times 100$$

$$\text{\% Non-viability} = \text{total number of non-viable cells per}$$
$$\text{aliquot/total cells in an aliqoute} \times 100$$

2.7. Characterization of TMX-AG-INPs. To test the chemical features of TMX-AG-INPs, AG-INPs, INPs, and

TMX alone, Fourier-transform infrared (FTIR) spectroscopy (IRTracer-100 Shimadzu) was used. FTIR spectrum was determined between 4000 and 500 cm^{-1} in the transmittance mode. Transmission electron microscopy (TEM) was used to determine the size, shape, and morphology of all nanoparticles. Images were recorded using a JEM-2100 (JEOL, Japan) with 200 kV energy, 1,500,000× magnification, and 1.4 Å resolving power. Surface properties were analyzed using scanning electron microscopy (SEM; KYKY-EM6900). The XRD (X-ray powder diffraction) was used to determine crystallographic patterns by the X-ray diffractometer JEOL, Japan, model JDX-3532, using 20−40 kV voltage, 2.5−30 mA current, Cu K$_\alpha$ (wavelength = 1.5418 Å) X-rays, and the 0−160° 2θ-range.

2.8. Chemicals and Media. The green tea extract (commercial tea retailer Islamabad), CYTIVA Whatman fluted filter paper, grade 5V (Thomas Scientific), ferric chloride hexahydrate (FeCl$_3$·6H$_2$O, Sigma-Aldrich, cat no. 236489), agar (Merck, Millipore cat no. 101614), NaOH (sodium hydroxide) (Merck, Millipore cat no. 106462), tamoxifen citrate salt (Sigma-Aldrich, cat no. T9262), MCF-7 (CLS cell line service no. 330273), PBS (phosphate buffered solution) (Sigma-Aldrich, cat no. P5244), DMEM (Gibco, cat no. 12320032), FBS (Gibco, cat no. 26140079), glutamine (Gibco, cat no. 21051024), trypsin (MERCK, cat no. 9002-07-7), and Trypan blue (MERCK, cat no. 72-57-1).

2.9. Media Used for Cell Culture. In low glucose DMEM (Gibco, cat no. 12320032), which contains 10% FBS (Gibco, cat no. 26140079), 2 mM glutamine (Gibco, cat no. 21051024), 0.01 mg/mL insulin, and 1% penicillin/streptomycin mix, MCF-7 human breast cancer cells were seeded at a density of 1×10^6 cells and then incubated at 37 °C in an atmosphere of 5% CO$_2$ (ESCO, CCL-240B-8-UV-WJ).

3. RESULTS

3.1. Characterization of TMX-AG-INPs. *3.1.1. FTIR Analysis.* The chemical structure of the iron nanoparticles (INPs, Figure 1A) was not affected by agar coating (AG-INPs, Figure 1B), as they both have the same H-bond stretches at 3600 cm^{-1}, C−C triple bond stretches at 2300 cm^{-1}, C=O at 15−1600 cm^{-1} and C−O stretching vibrations were found at 1200 cm^{-1}. Thus, the INPs maintain their molecular bonds and stability even after the carbohydrate (agar) coating (AG-INPs).

The FTIR spectra of iron nanoparticles loaded with the drug tamoxifen (TMX-AG-INPs, Figure 1D) show several small peaks, indicating the complex nature of the molecule. The FTIR spectra shows OH-stretching at 3600 cm^{-1}, intra molecular H-bonds at 3400 cm^{-1}, CH stretching at 3200 cm^{-1}, N−H stretch at 3118 cm^{-1}, N−CH$_3$ (aromatic) stretch at 2949 cm^{-1}, C=N stretching vibration at 2500 cm^{-1}, amide II at 1525 cm^{-1}, C−O−C stretch vibration at 1205 cm^{-1}, and CH=CH (cis) at 600 cm^{-1}. The TMX-AG-INPs show a different FTIR spectrum than tamoxifen (Figure 1C) alone.

3.1.2. Morphological Analysis by SEM. The structure, morphology, and texture of the AG-INPs and TMX-AG-INPs surfaces were determined by using scanning electron microscopy Figure 2. The SEM images of the Ag-INPs (Figure 2A) and TMX-Ag-INPs (Figure 2B) show an amorphous structure with a rough surface as they are agglomerated and stuck to each other because of the agar coating. It makes their surface rough and coarse. The particle size as determined by ImageJ software was in the range of 26−88 nm. The size of
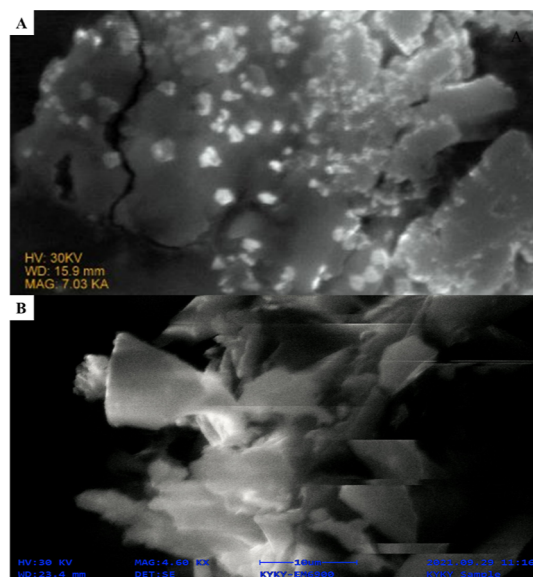

Figure 2. Scanning electron micrograph of (A) INPs and (B) TMX-AG-INPs.

TMX-AG-INPs was different (avg. size 32.1 nm), and the dispersion of the particles was greatly improved.

The particle size distribution was calculated by the ImageJ software, and a histogram of the particle size distribution is given in Figure 3. We obtained a unimodal with no gap. The
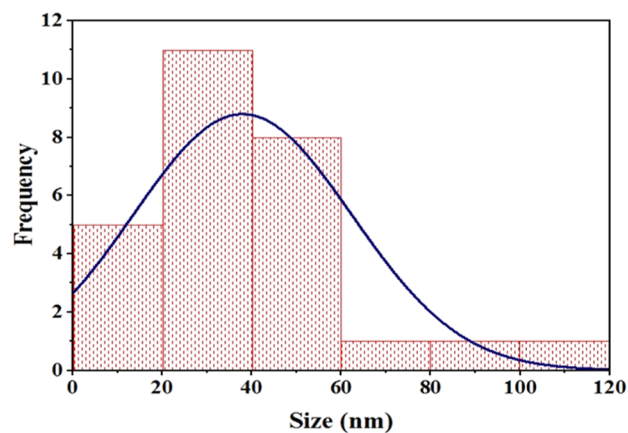

Figure 3. Histogram representing the particle size distribution of the iron nanoparticles. The *X*-axis indicates the particle size in nm, and the *Y*-axis represents the frequency of intervals.

particle size distribution was studied statistically by using the Gaussian function as follows

$$y = y_0 + \frac{A\ e^{-4\ln(2)(x-x_c)^2/W^2}}{\sqrt{\frac{\pi}{4\ln(2)}}}$$

where y_0 = base, x_c = center, A = area, and W = FWHM (**full width at half maximum**).

The average particle size determined (x_c) was 26.8 nm with a 0.15 standard error, the base (y_0) was 1.58 with a 0.05 standard error, the area A of the overall distribution peak was 402 with a 5.7 standard error, and exact individual particle size W (FWHM) was 32 nm with a 0.43 standard error. The reduced χ^2 was 1.69, and R^2 (COD) was 0.90. Table 1

Table 1. Statistical Evaluation of TMX-AG-INPs

	value	standard error	t-value	prob > |t|	dependency
y_0	1.15708	0.05946	19.45953	1.00362×10^{-71}	0.52194
x_c	26.73971	0.15591	171.50359	0	0.00562
A	402.56324	5.73634	70.17771	0	0.6969
W	32.56124	0.4336	75.09565	0	0.50942

represents the details of the statistical evaluation of TMX-AG-INPs.

3.1.3. Morphological Analysis by TEM. The structure and texture of TMX-AG-INPs were also determined by electron microscopy (Figure 4). The average particle size of TMX-AG-
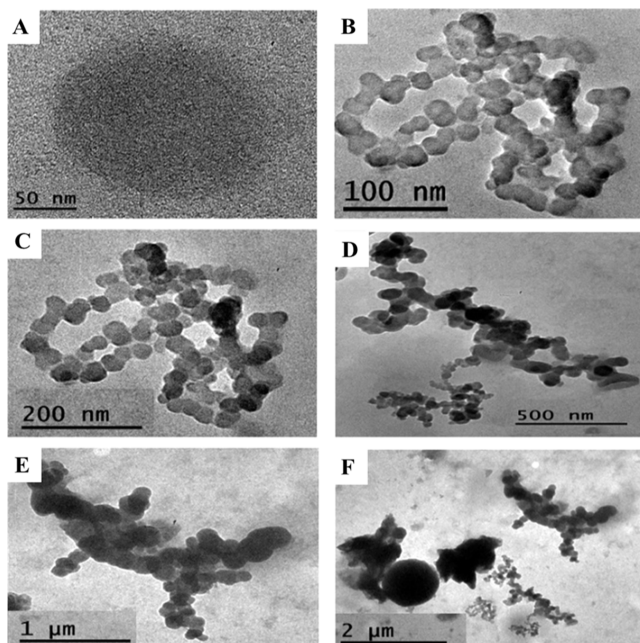
Figure 4. Electron micrographs of TMX-AG-INPs at various resolutions ranging from 50 nm (A) to 2 μm (F). The bar at the base represents the scale.

INPs (x_c) was 32.1 nm with 0.33 standard error, the base (y_0) was 1.37 with 0.32 standard error, the area A of the overall distribution peak was 98.24 with 9.6 standard error, and the exact individual particle size W (FWHM) was 10 nm with 0.56 standard error. The reduced χ^2 was 0.56, and R^2 (COD) was 0.97. A detailed statistical evaluation is given in Table 2. Figure

Table 2. Statistical Evaluation of TMX-AG-INP Size Distribution Using TEM Analysis

	value	standard error	t-value	prob > |t|	dependency
y_0	1.37231	0.32888	4.17267	0.00872	0.42178
x_c	32.10357	0.33822	94.91824	2.45059×10^9	0.00733
A	98.2427	9.61543	10.2172	1.45196×10^4	0.6038
W	9.7143	0.74502	11.69677	8.02696×10^5	0.44545

4 represents the morphology of TMX-AG-INPs at various resolutions (50, 100, 200, and 500 nm, as well as at 1 and 2 μm; Figure 4A–F respectively). Figure 5 represents the average particle size of TMX-AG-INPs.

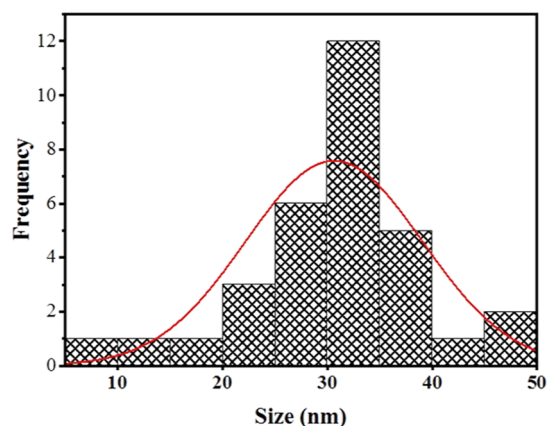*3.1.4. X-ray Powder Diffraction.* The XRD patterns clearly depict the amorphous structure of both the Ag-INPS and

Figure 5. Histogram of particle size distribution of TMX-AG-INPs, as measured by TEM analysis. The *X*-axis shows the size of nanoparticles on the nm scale, whereas the *Y*-axis represents the frequency of intervals.

TMX-AG-INPs, represented by a single prominent diffraction peak in the 2θ range at 19.02 and 20.86°, respectively (Figure 6A,B). The crystallinity of a sample is expressed by its crystallinity index (CI). The percent crystallinity index of AG-INPs was 9.6, and that of TMX-AG-INPs was 12.5, as calculated using the following formula

$$CI \% = total \ area \ of \ the \ crystalline \ peaks / total \ area \ of$$

$$crystalline \ and \ amorphous \ peaks \times 100$$

3.2. *In Vitro* **Drug Release Profile.** The entrapment efficiency of the TMX-AG-INPs was recorded at 88%, and the DL capacity was 43.5%. The total amount of the drug released was proportional to the concentration (c) of a sample, the length of the path (b) (cm) (the longer the path length, the more molecules in the path of the radiation beam, and thus the absorbance increases), and the molar absorptivity (ε) (mol/L). This allows the construction of the Beer−Lambert law graph ($A = \varepsilon bc$) (Figure 7A). This expresses the relationship between concentration, route length, and molar absorptivity that is directly proportional to absorbance (Figure 7A). A graph representing the release of the drug with time is given in Figure 7B, where the *X*-axis gives time and the *Y* axis gives the percentage of drug released. The overall drug release was determined using Beers law: $A = \varepsilon bc$. Drug release was measured at pH 7.4 for 12 h *in vitro*. The release of the drug was steady over time. In the first 6 h, around 50% of the drug was released, whereas in 12 h, 99% of the drug was released from nanoparticles. The cumulative drug release profile of TMX-AG-INPs is shown in Table 3. The highest cumulative drug release of TMX-AG-INPs after 12 h was noted as 19.8 mg.

3.3. *In Vitro* **Anti-cancer Activity of TMX-AG-INPs.** To check anti-cancer activity, six different concentrations of TMX-AG-INPs in 0.1 M PBS were used on the MCF-7 cancer cell
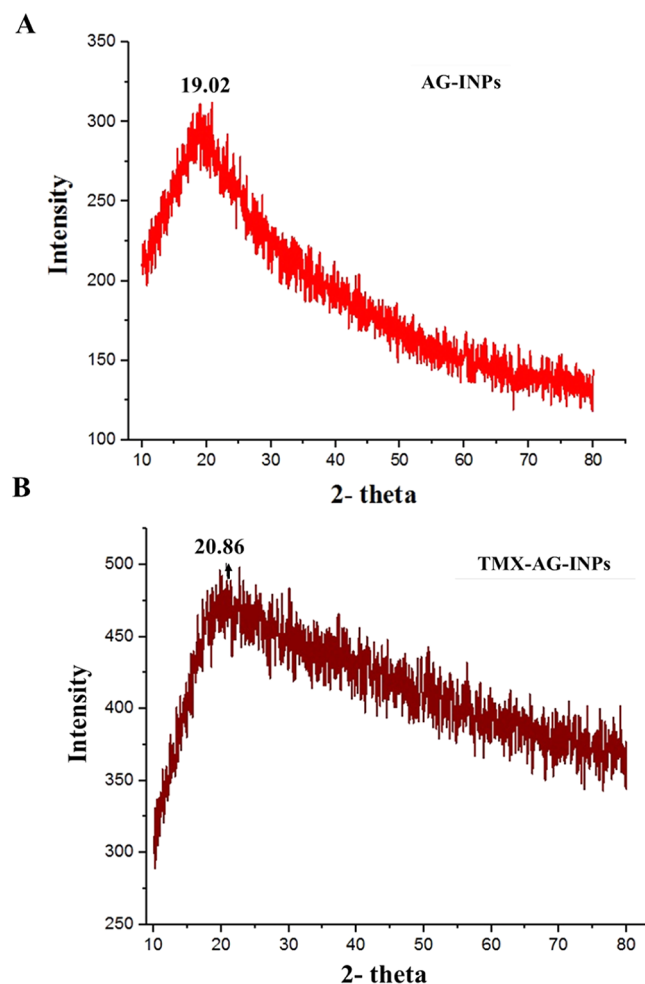
Figure 6. X-ray diffraction pattern of AG-INPs (A) and TMX-AG-INPs (B).

Figure 7. (A) Relationship of absorption, molar concentration, and path length of beam; (B) percentage of drug released over a 12 h period.

line. Tamoxifen alone (TMX) and AG-INPs were used as controls at the same concentrations (Figure 8). The percentage of non-viable cells in AG-INPs increased as the concentration of the particles increased (84% viable cells at 10 mg *vs* 47% viable cells at 60 mg). However, these values were significantly lower than TMX-AG-INPS and TMX alone ($p = 0.001$ and $p = 0.001$, respectively) indicating the efficient killing by tamoxifen. The TMX-AG-INPs were significantly more efficient in killing MCF-7 cells in comparison to TMX alone, as indicated by significantly more non-viable cells in the TMX-AG-INPs treatment group for all six concentrations. The statistical significance in terms of p values at different concentrations is given in Table 4. Results indicate that the efficiency of TMX-AG-INPs was higher than that of TMX alone at all concentrations (Figure 8, Table 5).

4. DISCUSSION

Tamoxifen (TMX) is widely used in the treatment of breast cancer; however, like most cancer therapy drugs that cause severe damage to normal cells as well, tamoxifen also has its side effects. Tamoxifen induces endometrial and liver cancer, which limits its long-term therapeutic use.[9,18] The major side effects of TMX are dose- and concentration-dependence. These side effects can be overcome by dosage maintenance over a course of time.
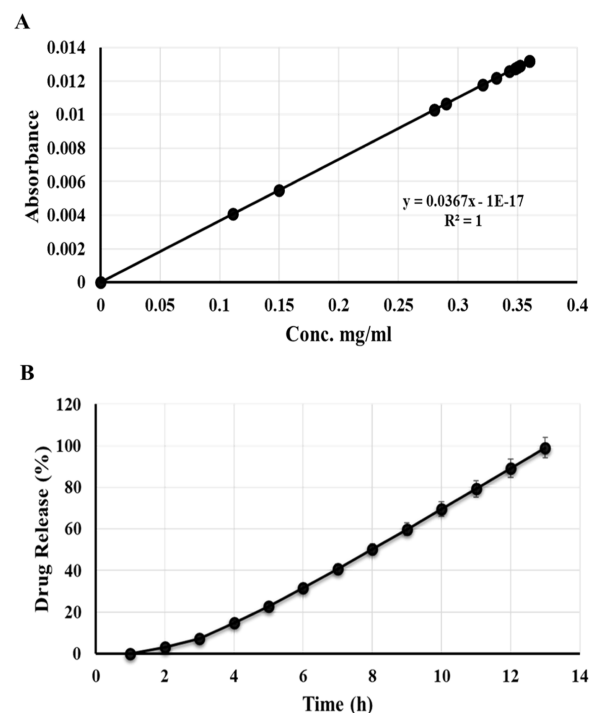
Nanotechnology has helped a lot to deliver these therapeutic drugs directly to the cancer tissues, specifically preventing serious damage to healthy tissue.[10] It can lead to improved clearance of drugs from the body, increased bioavailability, targeted delivery of conjugated drugs to cancer tissue, increased efficacy, slow release, and hence dose maintenance. Many nanocarrier systems have been employed to carry TMX molecules and deliver them selectively to solid breast tumors with high accuracy and little off-target side effects, utilizing the favorable aspects of the drug while eliminating cytotoxicity due to non-targeted delivery.[9,10,19]

Iron oxide nanoparticles also have proven their utility for cancer treatment. When synthesized with chemical methods, they have a lower cost of production and a high yield.[20] INPs are extensively used as nanocarrier systems to deliver several chemotherapy drugs for breast cancer treatment. As such, dextran-coated INPs were used to carry miR-29a (micro-RNA) to the breast cancer tissue with improved delivery, causing downregulation of anti-apoptotic genes.[21] In another study, INPs combined with gold nanoparticles were conjugated with bovine albumin, resulting in antitumor effects on MCF-7 and SKBR3 breast cancer cell lines, causing efficient cell death and apoptosis.[22] A few other drugs, such as methotrexate (MTX) and doxorubicin, have also been shown to deliver efficiently when combined with INPs. They have been proven safe by several studies in the past, and they have also been demonstrated to enhance the effect of nanocarriers and drug delivery to cancer tissues.[23]

The current study was designed to synthesize INPs with green tea extract using the co-precipitation method, which is widely used because of its good efficacy. This extract acts as a natural oxidizing agent. Moreover, they were coated with agar, a polymeric carbohydrate that can easily be degraded and processed in the human body. Agar is a jelly-like polymer that

Table 3. Drug Release Profile TMX-AG-INPs

| time (h)	absorbance	concentration (mg/mL)	dilution factor	concentration (mg/30 mL)	cumulative drug release (mg)
0	0	0	0	0	0
1	0.111	0.004074591	0.020372954	0.611188606	0.611
2	0.15	0.005506204	0.027531018	0.825930548	1.436930548
3	0.28	0.010278247	0.051391234	1.541737024	2.978667572
4	0.29	0.010645327	0.053226635	1.59679906	4.575466632
5	0.321	0.011783276	0.058916379	1.767491374	6.342958006
6	0.332	0.012187064	0.06093532	1.828059614	8.17101762
7	0.343	0.012590852	0.062954262	1.888627854	10.05964547
8	0.348	0.012774392	0.063871962	1.916158872	11.97580435
9	0.35	0.012847809	0.064239043	1.92717128	13.90297563
10	0.352	0.012921225	0.064606123	1.938183687	15.84115931
11	0.36	0.013214889	0.066074444	1.982233316	17.82339263
12	0.36	0.013214889	0.066074444	1.982233316	19.80562595
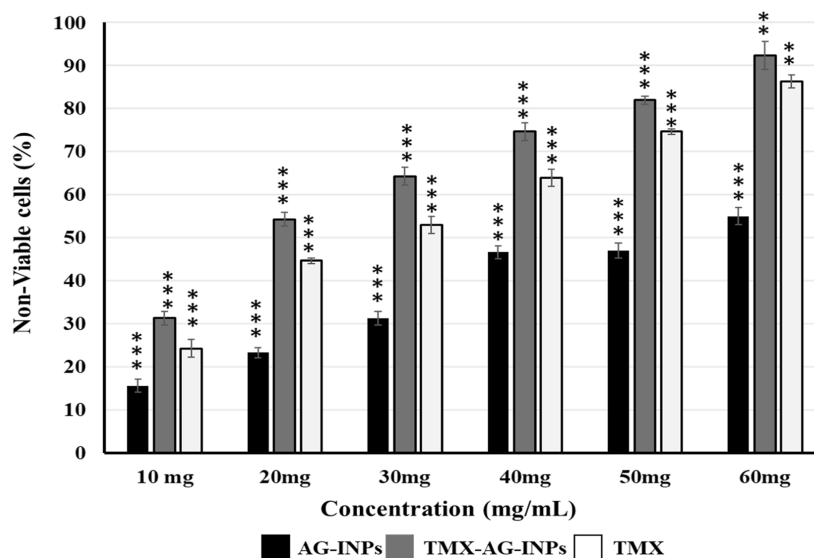
Figure 8. Graph representing non-viable MCF-7 cell lines after treatment with various concentrations of AG-INPS, TMX, and TMX-AG-INPs. * Represents significance. The *X*-axis indicates the concentration of nanoparticles, whereas the *Y*-axis indicates the percentage of non-viable cells determined by the dye exclusion test.

Table 4. Statistical Probability, as Determined by Two-Way ANOVA Analysis[a]

concn (mg)	INPs *vs* TMX p value	TMX-AG-INPs *vs* INPs p value	TMX *vs* TMX-AG-INPs p value
10	<0.001	<0.001	<0.00322
20	<0.001	<0.001	<0.001
30	<0.001	<0.001	<0.001
40	<0.001	<0.001	<0.001
50	<0.001	<0.001	<0.00158
60	<0.001	<0.001	<0.0263

[a]Values are indicated by * in Figure 8.

has two components: agarose and agaropectin. Due to its non-toxicity and biodegradability, it is a common choice in the pharmaceutical industry for gels, tablets, and nanocarrier systems. It can make hydrogels for the controlled release of drug. Moreover, coating agar on nanoparticles increases the available surface area and hence the entrapment of the drug.[24]

The entrapment efficiency (EE) of the TMX-AG-INPs in the current study was 88% with a DL capacity of 43.5%. A study utilizing INPs loaded with protein (tyrosine amino acid) conducted by Nosrati *et al.* reported 51.21% EE of INPs and 11.34% DL for tamoxifen loaded on to tyrosine-encoded magnetic nanoparticles,[15] which is less than the current study.

Table 5. Viable Cells after Treatment with TMX-AG-INPs

concn (mg)	viability (%)	non-viability (%)	viable cells/square	non-viable cells/square	viable cells/mL	non-viable cells/mL
10	68	31	68	31	1.375×10^6	6.25×10^5
20	47	53	35	40	7.0×10^5	8.0×10^5
30	35	65	21	39	4.25×0^5	7.75×10^5
40	26	74	26	74	5.2×10^5	1.48×10^5
50	18	81	14	61	2.75×10^5	1.225×10^7
60	10	90	6	54	1.2×10^5	1.08×10^6

However, Heidari Majd *et al.* found 49.1% DL of tamoxifen-loaded folic acid-armed PEGylated magnetic nanoparticles,[25] which is 6% greater than the present study. It may be suggested that complex carbohydrates may provide better entrapment of the drug. Moreover, recently, the TMX loading efficiency in tamoxifen-loaded biocompatible hybrid magnetic nanoplatforms was found to be less than 60% by Cadena Castro *et al.*[26] Drug loading was found to be directly proportional to the amount of the drug added during the preparation of the different formulations, up to an approximate drug.

The size and morphology of the TMX-AG-INPs were appropriate (20−90 nm). Particles smaller than 1 μm can pass through vasculature easily and exhibit better accumulation in cancer tissues due to enhanced vascularity. Smaller particles can easily pass through the membranes and accumulate differently in tumor tissue. Particles in the size range of 40−100 nm are better taken up by cells by endocytosis than larger particles.[27] After treatment of MCF-7 cells with TMX-AG-INPs, the percentage of viable cells decreased with increasing concentrations of particles, as determined after 48 h of incubation with various concentrations of TMX-AG-INPs. The selected concentration of tamoxifen was in line with the recommended average daily dosage of the drug for patients, 20−40 mg.[28] The percentage of non-viable cells for the TMX-AG-INPs-treated group was comparable to TMX alone. It was in agreement with a study reported by Rostami *et al.*, where tamoxifen-loaded lysin-coated nanoparticles were found equally significant in controlling cell proliferation, as indicated by cell viability assays. In view of this, it is safe to suggest that TMX-AG-INPs are good candidates for breast cancer control evaluation after further studies.[29]

5. CONCLUSIONS

TMX-AG-INPs were produced in this study, and they exhibited optimum hydrodynamic diameter and had good entrapment efficacy for the drug tamoxifen. These particles were able to release drugs efficiently and consistently over a 12 h period. Moreover, cell viability assays indicated they were equally good at controlling breast cancer cell line MCF-7 proliferation *in vitro*, indicating their potential as nanocarriers; however, to warrant their use as nanodrug carriers, they need *in vivo* experimental analysis.

■ AUTHOR INFORMATION

Corresponding Author

    Nazish Bostan − *Molecular Virology Labs, Department of Biosciences, COMSATS University Islamabad, Islamabad 45550, Pakistan;* ● orcid.org/0000-0003-2226-5440; Email: nazishbostan@comsats.edu.pk

Authors

    Zanib Khan − *Molecular Virology Labs, Department of Biosciences, COMSATS University Islamabad, Islamabad 45550, Pakistan*

    Sadia Sattar − *Molecular Virology Labs, Department of Biosciences, COMSATS University Islamabad, Islamabad 45550, Pakistan*

    Muhammad Abubakar − *National Veterinary Laboratory, National Agricultural Research Centre, Islamabad 45300, Pakistan*

    Muhammad Javed Arshed − *National Veterinary Laboratory, National Agricultural Research Centre, Islamabad 45300, Pakistan*

    Roohi Aslam − *Department of Biology, NUTECH, Islamabad 44000, Pakistan;* Present Address: Atta ur Rehman School of Applied Biosciences, National University of Science and Technology, Islamabad

    Syed Tahir Abbas Shah − *Functional Genomics Lab, Department of Biosciences, COMSATS University Islamabad, Islamabad 45550, Pakistan;* ● orcid.org/0000-0001-9151-9374

    Sundus Javed − *Microbiology and Public Health Laboratory, Department of Biosciences, COMSATS University Islamabad, Islamabad 45550, Pakistan*

    Aamira Tariq − *Microbiology and Public Health Laboratory, Department of Biosciences, COMSATS University Islamabad, Islamabad 45550, Pakistan*

    Shumaila Manzoor − *National Veterinary Laboratory, National Agricultural Research Centre, Islamabad 45300, Pakistan*

Complete contact information is available at:
https://pubs.acs.org/10.1021/acsomega.3c00844

Author Contributions

Dr. Nazish Bostan (experimental design, supervision, and funding). Dr. Muhammad Javed Arshed and Dr. Muhammad Abu Bakar (Experimental design, Funding, and logistic support). Zanib Khan (experimental work and paper writing initial draft). Dr. Sadia Sattar (Data analysis, final manuscript preparation, data curation, and presentation). Dr. Roohi Aslam, Dr. Sundus Javed, Dr. Amira Tariq, and Ms. Shumaila Manzoor (manuscript revision and data verification). Dr. Tahir Abbas Shah (statistical analysis).

Notes

The authors declare no competing financial interest.

■ ACKNOWLEDGMENTS

■ REFERENCES

(1) Malvezzi, M.; Carioli, G.; Bertuccio, P.; Boffetta, P.; Levi, F.; La Vecchia, C.; Negri, E. European cancer mortality predictions for the year 2019 with focus on breast cancer. *Ann. Oncol.* **2019**, *30*, 781−787.

(2) Peart, O. Breast intervention and breast cancer treatment options. *Radiol. Technol.* **2015**, *86*, 535M−558M.

(3) Al-Mahayri, Z. N.; Patrinos, G. P.; Ali, B. R. Toxicity and Pharmacogenomic Biomarkers in Breast Cancer Chemotherapy. *Front. Pharmacol.* **2020**, *11*, 445.

(4) Sinha, R.; Kim, G. J.; Nie, S.; Shin, D. M. Nanotechnology in cancer therapeutics: Bioconjugated nanoparticles for drug delivery. *Mol. Cancer Ther.* **2006**, *5*, 1909−1917.

(5) Cuzick, J.; Sestak, I.; Cawthorn, S.; Hamed, H.; Holli, K.; Howell, A.; Forbes, J. F. Tamoxifen for prevention of breast cancer: Extended long-term follow-up of the IBIS-I breast cancer prevention trial. *Lancet Oncol.* **2015**, *16*, 67−75.

(6) Harper, M. J.; Walpole, A. L. A new derivative of triphenylethylene: effect on implantation and mode of action in rats. *J. Reprod. Fertil.* **1967**, *13*, 101−119.

(7) Gharebaghi, F.; Dalali, N.; Ahmadi, E.; Danafar, H. Preparation of wormlike polymeric nanoparticles coated with silica for delivery of

methotrexate and evaluation of anticancer activity against MCF-7 cells. *J. Biomater. Appl.* **2017**, *31*, 1305−1316.

(8) Day, C. M.; Hickey, S. M.; Song, Y.; Plush, S. E.; Garg, S. Novel tamoxifen nanoformulations for improving breast cancer treatment: Old wine in new bottles. *Molecules* **2020**, *25*, 1182.

(9) Jena, S. K.; Sangamwar, A. T. Polymeric micelles: A promising tool for tamoxifen delivery in cancer? *Ther. Delivery* **2017**, *8*, 109−111.

(10) Day, C. M.; Parikh, A.; Song, Y.; Garg, S. Nanotechnology and Nature's Miracle Compound: Curcumin. In *NanoNutraceuticals*; CRC Press, 2018.

(11) Xuan, Q. J.; Wang, J. x.; Nanding, A.; Wang, Z. p.; Liu, H.; Lian, X.; Zhang, Q. y. Tumor-associated macrophages are correlated with tamoxifen resistance in the postmenopausal breast cancer patients. *Pathol. Oncol. Res.* **2014**, *20*, 619−624.

(12) Ventola, C. L. Progress in Nanomedicine: Approved and Investigational Nanodrugs. *Pharm. Ther.* **2017**, *42*, 742.

(13) Dai, Y.; Xu, C.; Sun, X.; Chen, X. Nanoparticle design strategies for enhanced anticancer therapy by exploiting the tumour micro-environment. *Chem. Soc. Rev.* **2017**, *46*, 3830−3852.

(14) Sharma, A.; Jain, N.; Sareen, R. Nanocarriers for diagnosis and targeting of breast cancer. *BioMed Res. Int.* **2013**, *2013*, 1−10.

(15) Nosrati, H.; Rashidi, N.; Danafar, H.; Manjili, H. K. Anticancer Activity of Tamoxifen Loaded Tyrosine Decorated Biocompatible Fe3O4 Magnetic Nanoparticles Against Breast Cancer Cell Lines. *J. Inorg. Organomet. Polym. Mater.* **2018**, *28*, 1178−1186.

(16) Chevalier, M. T.; Rescignano, N.; Martin-Saldaña, S.; González-Gómez, Á.; Kenny, J. M.; San Román, J.; Mijangos, C.; Álvarez, V. A. Non-covalently coated biopolymeric nanoparticles for improved tamoxifen delivery. *Eur. Polym. J.* **2017**, *95*, 348−357.

(17) Jayashree, V.; Thenmozhi, N. In vitro anti-proliferative assay and cell viability activity of Baicalein using breast cancer cell line. *Int. J. Pharm. Sci. Res.* **2018**, *9*, 1620−1624.

(18) Kassem, M. A.; Megahed, M. A.; Abu Elyazid, S. K.; Abd-Allah, F. I.; Abdelghany, T. M.; Al-Abd, A. M.; El-Say, K. M. Enhancing the Therapeutic Efficacy of Tamoxifen Citrate Loaded Span-Based Nano-Vesicles on Human Breast Adenocarcinoma Cells. *AAPS PharmSci-Tech* **2018**, *19*, 1529−1543.

(19) Bhagwat, G. S.; Athawale, R. B.; Gude, R. P.; Md, S.; Alhakamy, N. A.; Fahmy, U. A.; Kesharwani, P. Formulation and Development of Transferrin Targeted Solid Lipid Nanoparticles for Breast Cancer Therapy. *Front. Pharmacol.* **2020**, *11*, 614290.

(20) Lorkowski, M. E.; Atukorale, P. U.; Ghaghada, K. B.; Karathanasis, E. Stimuli-Responsive Iron Oxide Nanotheranostics: A Versatile and Powerful Approach for Cancer Therapy. *Adv. Healthcare Mater.* **2021**, *10*, 2001044.

(21) Yalcin, S. Dextran-coated iron oxide nanoparticle for delivery of miR-29a to breast cancer cell line. *Pharm. Dev. Technol.* **2019**, *24*, 1032−1037.

(22) Baneshi, M.; Dadfarnia, S.; Shabani, A. M. H.; Sabbagh, S. K.; Haghgoo, S.; Bardania, H. A novel theranostic system of AS1411 aptamer-functionalized albumin nanoparticles loaded on iron oxide and gold nanoparticles for doxorubicin delivery. *Int. J. Pharm.* **2019**, *564*, 145−152.

(23) Sharma, G.; Kodali, V.; Gaffrey, M.; Wang, W.; Minard, K. R.; Karin, N. J.; Teeguarden, J. G.; Thrall, B. D. Iron oxide nanoparticle agglomeration influences dose rates and modulates oxidative stress-mediated dose–response profiles in vitro. *Nanotoxicology* **2014**, *8*, 663−675.

(24) Kandar, C. C.; Hasnain, M. S.; Nayak, A. K. Chapter 1— Natural polymers as useful pharmaceutical excipients. In *Advances and Challenges in Pharmaceutical Technology*; Nayak, A. K., Pal, K., Banerjee, I., Maji, S., Nanda, U., Eds.; Academic Press, 2021; pp 1−44.

(25) Heidari Majd, M.; Asgari, D.; Barar, J.; Valizadeh, H.; Kafil, V.; Abadpour, A.; Moumivand, E.; Mojarrad, J. S.; Rashidi, M. R.; Coukos, G.; et al. Tamoxifen loaded folic acid armed PEGylated magnetic nanoparticles for targeted imaging and therapy of cancer. *Colloids Surf., B* **2013**, *106*, 117−125.

(26) Cadena Castro, D.; Gatti, G.; Martín, S. E.; Uberman, P. M.; García, M. C. Promising tamoxifen-loaded biocompatible hybrid magnetic nanoplatforms against breast cancer cells: synthesis, characterization and biological evaluation. *New J. Chem.* **2021**, *45*, 4032−4045.

(27) Dolai, J.; Mandal, K.; Jana, N. R. Nanoparticle Size Effects in Biomedical Applications. *ACS Appl. Nano Mater.* **2021**, *4*, 6471−6496.

(28) Lazzeroni, M.; Serrano, D.; Dunn, B. K.; Heckman-Stoddard, B. M.; Lee, O.; Khan, S.; Decensi, A. Oral low dose and topical tamoxifen for breast cancer prevention: modern approaches for an old drug. *Breast Cancer Res.* **2012**, *14*, 214.

(29) Rostami, S.; Tafvizi, F.; Kheiri Manjili, H. R. High efficacy of tamoxifen-loaded L-lysine coated magnetic iron oxide nanoparticles in cell cycle arrest and anti-cancer activity for breast cancer therapy. *Bioimpacts* **2022**, *12*, 301−313.